Electronic Supplementary Material (ESI) for Soft Matter.

SUPPLEMENTARY INFORMATION

Complex-type N-glycans on VSV-G pseudotyped HIV exhibit 'tough' sialic and 'brittle' mannose self-adhesions.

Running title: complex-type N glycans have tough and brittle sugar self-adhesions

Hashanthi K. Abeyratne-Perera[1], Eric Ogharandukun[2], Preethi L. Chandran PhD [2,1]

[1] Biochemistry and Molecular Biology Department, College of Medicine

[2] Chemical Engineering Department, College of Engineering and Architecture

Howard University, Washington DC.

Corresponding author

Preethi L. Chandran, PhD

Assistant Professor

Department of Chemical Engineering, College of Engineering and Architecture, Howard University

Department of Biochemistry and Molecular Biology, College of Medicine, Howard University

Address:

1011 LK Downing Hall

2300 6th Street, NW, Howard University

Washington, DC 20059.

Email: preethi.chandran@howard.edu

Phone: 202-806-4595

Supplementary Information 1

Dry AFM imaging and Dynamic Light Scattering studies were performed to assess the size and morphology of the pseudovirus at a population-level to check if it was in the range expected for wild-type HIV-1 virus.

Mica disks were pre-functionalized with (3-aminopropyl) triethoxysilane (APTES) by incubating them with freshly-prepared 1:100 dilution of 50 mM APTES solution for 30 minutes, followed by washing with MilliQ water and drying under a stream of N_2 gas. 6 µl of 1:300 dilutions of the 1x 10^7 /ml of viral titer of pseudovirus (kind gift of Dr. Sergei Nekhai at Howard University) in opti-MEM was placed on each APTES-mica and incubated for about five minutes, followed by washing with 1 ml water to remove unabsorbed virus and prevent salt crystallization on the surface. The washed surfaces were gently dried under a stream of N_2 gas. The dried virus adsorbed surfaces were imaged in the tapping mode of AFM (NS-V controller, Bruker Nano-surfaces, Inc., Santa Barbara, CA) with an OTESPA R3 cantilever (Bruker Inc., Billerica, MA). The cantilever deflection set point was lowered to exert a high force on the sample to image the capsid structure inside the viral envelopes. The virus diameter distribution was obtained from the nanoscope analysis software based on the dry AFM images.

In some instances, especially when imaging was done with high tapping forces, a population of viruses with irregular envelopes of variable sizes and shapes was observed (Suppl. Fig. 1A, left). In corresponding color-mapped height images, one could distinguish membrane boundaries (green) with one or more cone-shaped structures inside (purple), which could be attributed to the HIV-1 capsids protruding under the membrane (Suppl. Fig. 1A, right) [1, 2]. The cross-sectional height profile across a virus with multiple capsids (particle i in Suppl. Fig. 1) indicated a continuous membrane between capsid protrusions (Suppl. Fig. 1B, black arrow). The height profiles of several viruses had step increases (see red arrows in Suppl. Fig. 1B), which is expected when the underlying structure is layered. The morphology of this population of adsorbed pseudoviruses could be a representation of the membranous-bag-containing-multiple-capsids description ascribed to a subpopulation of HIV-1 virus observed in cryo-electron tomography [1]. The authors of that study reported that suspensions of *env*$^-$ HIV-1 virus have a small multi-capsid sub-population, which could not be ascribed to sample-processing or membrane-fusion artifacts [1]. While these high-force AFM scans in Suppl. Fig. 1A were useful to confirm the underlying HIV-like organization of the pseudovirus, under regular conditions and in

most cases we imaged a more 'conventional' population of pseudoviruses that were relatively homogenous in size and had more or less spherical shapes (Suppl. Fig. 1C). The tops of several of these surface-adsorbed viruses had flattened dents (blue arrow in height profile of Suppl. Fig. 1B, and inset of Suppl. Fig. 1C), suggesting an underlying shell structure that is collapsed. The area diameter D_A (i.e. the diameter of the adsorbed area of each virus) of the virus population was distributed between 78 - 166 nm, with a prominent peak at ~94 nm (Suppl. Fig. 1D, left). This diameter range encompasses that documented for the wild-type HIV-1 using electron microscopy: 90-160 nm [3], and 95-175 nm [4]. Since the long-side of the HIV-1 capsid has been reported to be ~100 nm [1, 2], we expect the virus population clustering around a D_A of 94 nm to mostly have only one capsid inside the membrane [5].

In Dynamic Light Scattering (DLS) studies, the virus suspension predominantly showed a single population of diffusing sizes (inferred from the single sharp exponential fall of the correlation curve) (Suppl. Fig. 1D right). The average hydrodynamic diameter D_H (i.e. the diameter of a stokesian sphere diffusing at the same speed as the virus) of the population was ~200nm, which is 2 times higher than the D_A (Suppl. Fig. 1C). The higher value of D_H can be because of the presence of a swollen glycan shield on suspended viruses but not on air-dried ones, and the consequent slowing down of the former's diffusion speed.

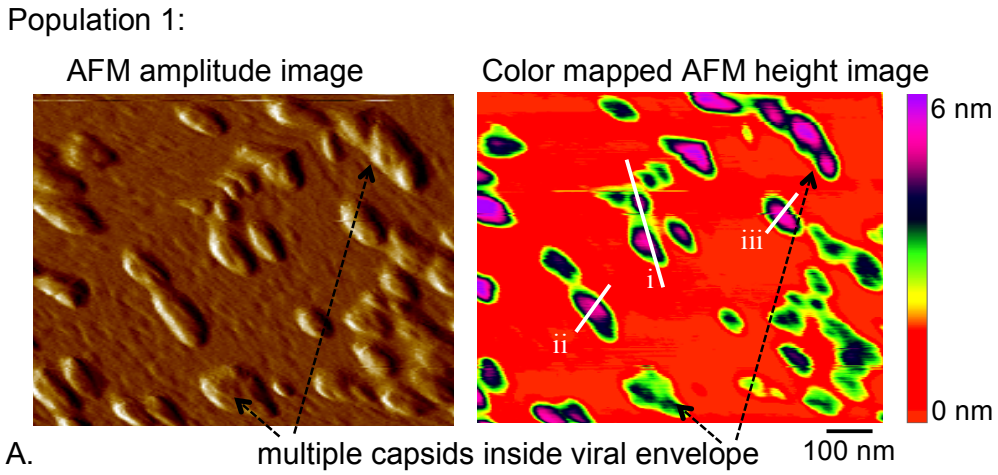

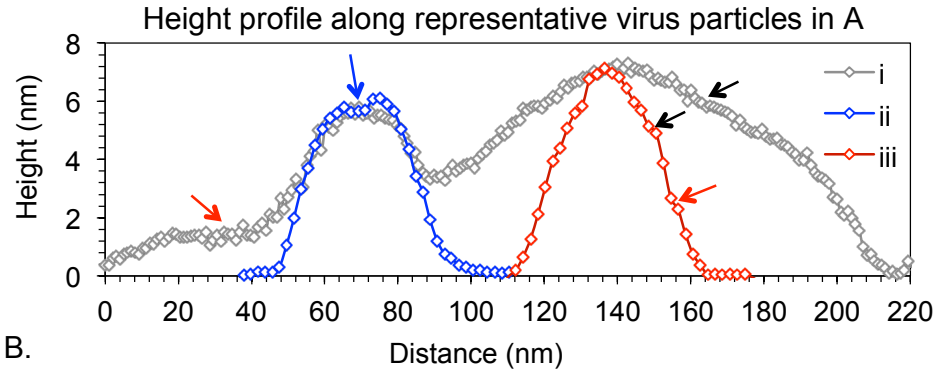

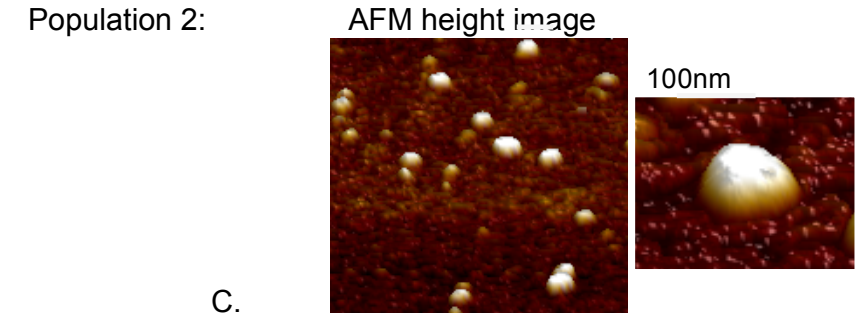

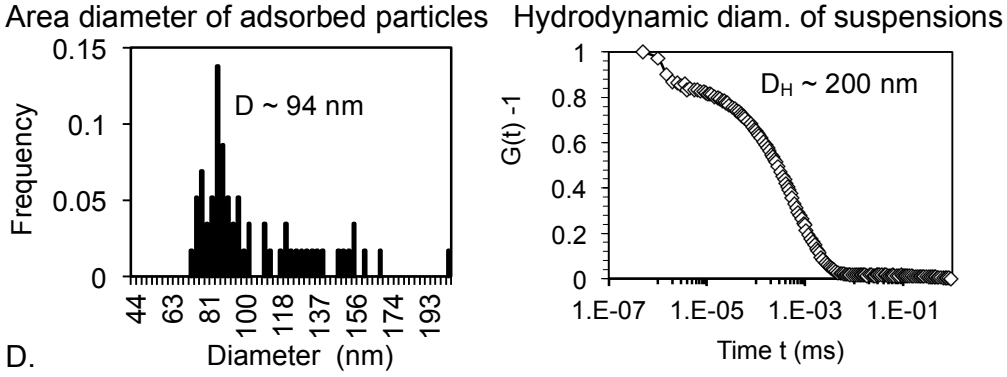

Figure 1: Morphology of HIV pseudovirus populations observed with AFM and DLS.

(A) Amplitude (left) and color-mapped height (right) images of one population of surface-adsorbed and air-dried pseudovirus scanned in AFM with relatively high force. Three height ranges corresponding to the surface (red), membrane (green), and encased capsids (purple) can be distinguished in the color-mapped images, with multiple conical capsids sometimes found encased within the pliable membrane envelopes. (B) Height profile along three representative virus particles in A that capture signature features. Particle i has two protrusions corresponding to two capsids present within a continuous membrane. Particles ii and iii are two particles having a single protruding capsid. Sharp height transitions possible between membrane-only (red arrows) and protruding capsid (black arrows) regions were seen in many cases. Several virus tops had small dips (blue arrows) possibly due to dented capsids. (C) Height images of a seemingly second population of surface-adsorbed pseudoviruses imaged in dry air with AFM, with a zoomed-in 3D rendering of a particle shown alongside. (D) Distribution of area diameters D_A (diameter of the area footprint of surface-adsorbed particles) obtained using image analysis of AFM height scans (left) and the DLS correlation curve of suspended virus particles from which a hydrodynamic diameter D_H of ~200nm is calculated (right).

Supplementary Information 2

A. Sugar-sugar self-interactions in 0mM NaCl

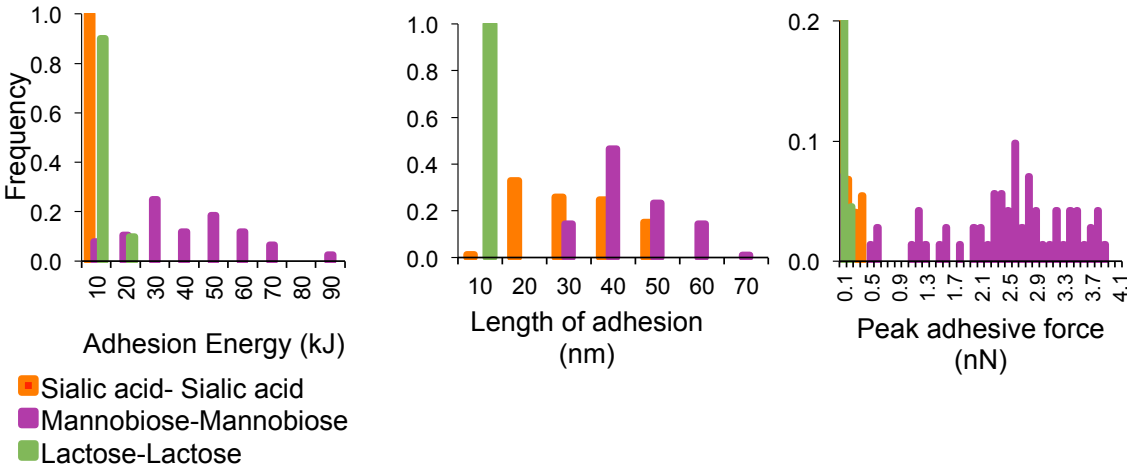

B. Sugar-sugar self-interactions in 150mM NaCl

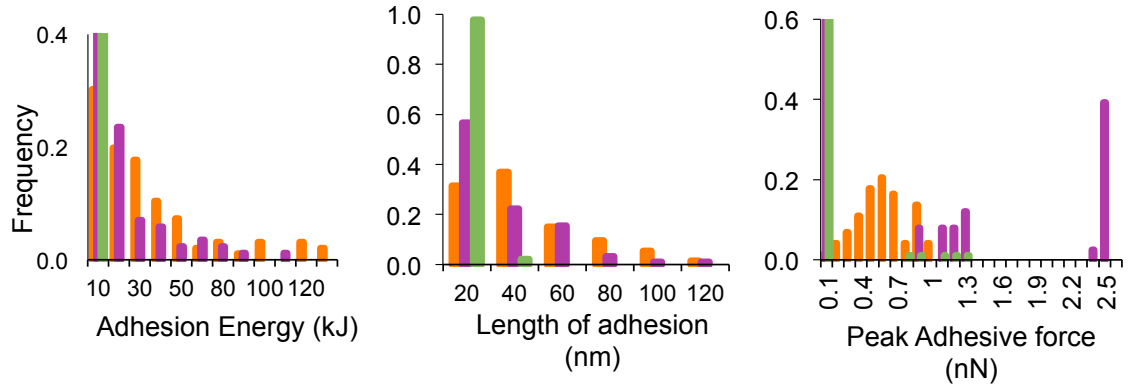

Histograms summarizing the adhesion features when two opposing monolayers of the same sugars are brought in contact and retracted. The self-adhesion of mannobiose monolayers is released with a strong peak force as the two surfaces lose physical contact (i.e. length of adhesion tends towards lower values). These principles hold for mannobiose self-adhesion in water and in the presence of salt, though the occurrences of peak forces is reduced with salt supplementation and gets distributed towards lowers magnitude. SA residues do not manifest self-adhesion in the absence of salt, due to the charge repulsion between the layers. All three markers of adhesion (adhesion energy, length of adhesion, and peak adhesive forces) are distributed on the lower end of the range for SA monolayers in water (top panel). In the

presence of salt (lower panel), however, SA monolayers show similar distribution of adhesion energy to mannobiose-monolayers, but the mechanism is different. While the peak forces for SA-SA self-adhesion are distributed towards smaller values than mannobiose self-adhesion, the lengths of adhesion are longer, with modal values ranging 3 – 4 times the physical distance of the two monolayers. The low-force but long-range characteristic of SA-SA interactions give more suppleness and malleability to these adhesions compared to mannobiose self-adhesions. To provide a good resolution of the data distribution, the scales were not kept constant between the two salt conditions.

Supplementary Information 3

In Abeyratne-Perera et al.[6] we showed that there are no significant interactions between monolayers of mannobiose and lactose in 0mM NaCl. There were no significant interactions between mannobiose and lactose monolayers in 150mM NaCl either (n ~ 100 force curves). A representative force curve was shown.

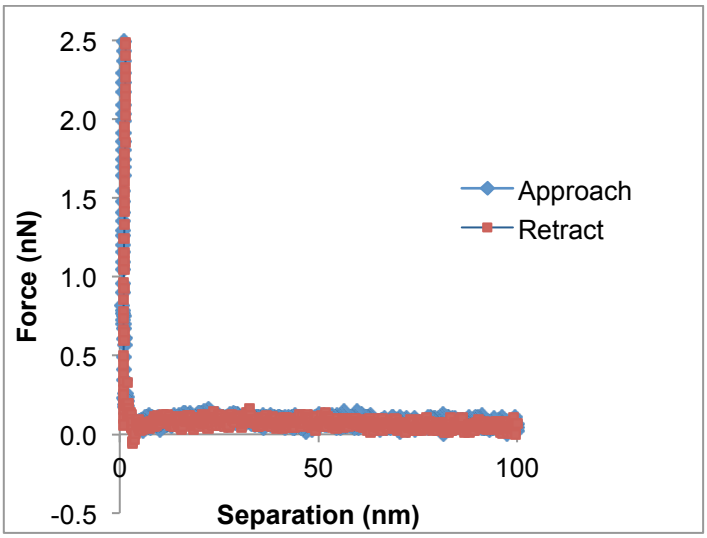

Supplementary Information 4

Control for enforced-contact force-spectroscopy studies:
AFM probes bearing only monolayers of linker molecules do not penetrate or adhere to the virus glycan shield (Fig.1), suggesting that adhesions seen when sugars are attached to the linkers must arise from interactions between the sugars and the glycan shield.

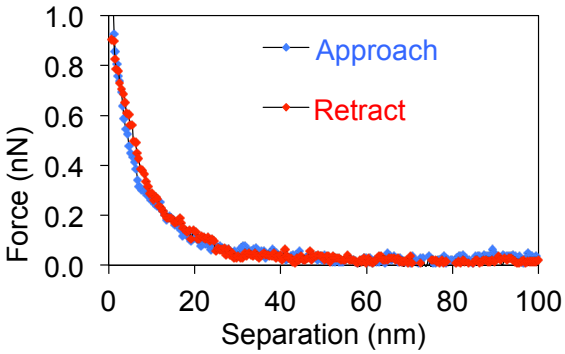

Figure 1:

Control for unenforced-contact nanoparticle studies:
Au Nanoparticles that were citrate-coated did not bind to the virus in solution. The control np solution did not show discernible color change (Fig. 2A), SPR shifts (Fig. 2B), or rightward shifts of the virus correlation curves signifying a size increase (Fig. 2C), when virus was added to the np solution.

Figure2: A.

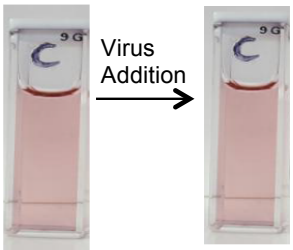

B.

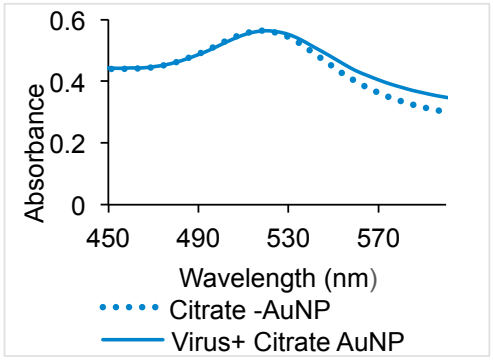

C.

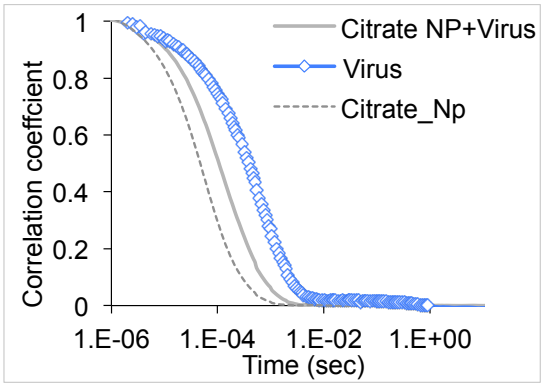

References:

1. G. A. Frank, K. Narayan, J. W. Bess, Jr., G. Q. Del Prete, X. Wu, A. Moran, L. M. Hartnell, L. A. Earl, J. D. Lifson and S. Subramaniam, *Nat Commun*, 2015, **6**, 5854.
2. G. Zhao, J. R. Perilla, E. L. Yufenyuy, X. Meng, B. Chen, J. Ning, J. Ahn, A. M. Gronenborn, K. Schulten, C. Aiken and P. Zhang, *Nature*, 2013, **497**, 643-646.
3. A. S. Reicin, A. Ohagen, L. Yin, S. Hoglund and S. P. Goff, *Journal of virology*, 1996, **70**, 8645-8652.
4. T. Dorfman, A. Bukovsky, A. Ohagen, S. Höglund and H. Göttlinger, *Journal of Virology*, 1994, **68**, 8180-8187.
5. J. A. Briggs, K. Grünewald, B. Glass, F. Förster, H.-G. Kräusslich and S. D. Fuller, *Structure*, 2006, **14**, 15-20.
6. H. K. Abeyratne-Perera and P. L. Chandran, *Langmuir*, 2017, **33**, 9178-9189.